Title
Spatial distribution of intracortical porosity varies across age and sex

Authors
Nirody, Jasmine A
Cheng, Karen P
Parrish, Robin M
et al.

Publication Date
2015-06-01

DOI
10.1016/j.bone.2015.02.006

Peer reviewed

HHS Public Access

Author manuscript

Bone. Author manuscript; available in PMC 2015 September 01.

Published in final edited form as:

Bone. 2015 June ; 75: 88–95. doi:10.1016/j.bone.2015.02.006.

Spatial distribution of intracortical porosity varies across age and sex

Jasmine A. Nirody[a], **Karen P. Cheng**[b,c], **Robin M. Parrish**[b], **Andrew J. Burghardt**[b], **Sharmila Majumdar**[b], **Thomas M. Link**[b], and **Galateia J. Kazakia**[b,*]

Jasmine A. Nirody: jnirody@berkeley.edu; Karen P. Cheng: kcheng329@berkeley.edu; Robin M. Parrish: rmparrish@berkeley.edu; Andrew J. Burghardt: andrew.burghardt@ucsf.edu; Sharmila Majumdar: sharmila.majumdar@ucsf.edu; Thomas M. Link: thomas.link@ucsf.edu; Galateia J. Kazakia: galateia.kazakia@ucsf.edu

[a]Biophysics Graduate Group, University of California, Berkeley, CA, USA

[b]Musculoskeletal Quantitative Imaging Research Group, Department of Radiology and Biomedical Imaging, University of California, San Francisco, CA, USA

[c]Department of Bioengineering, University of California, Berkeley, CA

Abstract

Cortical bone porosity is a major determinant of strength, stiffness, and fracture toughness of cortical tissue. The goal of this work was to investigate changes in spatial distribution and microstructure of cortical porosity associated with aging in men and women. The specific aims were to: 1) develop an automated technique for spatial analysis of cortical microstructure based on HR-pQCT data, and; 2) apply this technique to explore sex- and age-specific spatial distribution and microstructure of porosity within the cortex. We evaluated HR-pQCT images of the distal tibia from a cross-sectional cohort of 145 individuals, characterizing detectable pores as being in the endosteal, midcortical, or periosteal layers of the cortex. Metrics describing porosity, pore number, and pore size were quantifiedwithin each layer and compared across sexes, age groups, and cortical layers. The elderly cohort (65–78 years, n=22) displayed higher values than the young cohort (20–29 years, n=29) for all parameters both globally and within each layer. While all three layers displayed significant age-related porosity increases, the greatest difference in porosity between the young and elderly cohort was in the midcortical layer (+344%, $p < 0.001$). Similarly, the midcortical layer reflected the greatest differences between young and elderly cohorts in both pore number (+243%, $p < 0.001$) and size (+28%, $p < 0.001$). Females displayed greater age-related changes in porosity and pore number than males. Females and males displayed comparable small to non-significant changes with age in pore size. In summary, considerable variability exists in the spatial distribution of detectable cortical porosity at the distal tibia, and this variability is dependent on age and sex. Intracortical pore distribution analysis may ultimately provide insight into both mechanisms of pore network expansion and biomechanical consequences of pore distribution.

*Corresponding author at: Musculoskeletal Quantitative Imaging Research Group, Department of Radiology and Biomedical Imaging, University of California, San Francisco, 185 Berry St, Suite 350, San Francisco, CA 94107, USA. Fax: +1 415 353 9423.

Disclosures

AJB served on an advisory board for Amgen, was a paid consultant for Ultragenyx, and received royalties and travel support from Scanco Medical. SM has received grants from Merck and Amgen. JAN, KPC, RMP, TML, and GJK have nothing to disclose.

Keywords

Porosity; Cortical bone; Aging; Gender; HR-pQCT; Spatial distribution

Introduction

Cortical bone microstructure is vital to the mechanical competence and fracture resistance of long bones. Cortical bone porosity, in particular, is a major determinant of strength, stiffness, and fracture toughness of cortical tissue [1–3]. One recent study using HR-pQCT identified significant differences in cortical porosity in the ultradistal radius between young and elderly subjects matched for areal bone mineral density (aBMD) [4], suggesting that porosity contributes to the aBMD-independent effect of age on bone fragility and fracture risk [5]. This is supported by a second recent HR-pQCT study at the ultradistal radius in which cortical porosity predicted prevalent fractures independent of aBMD [6]. In addition to porosity, measures of pore structure including size, shape, orientation, and distribution may be critical in understanding fracture incidence [7,8].

Early studies of cortical pore distribution showed that porosity is not spatially uniform[9,10]; however, a lack of automated tools has limited the widespread implementation of spatial distribution analysis. More recent studies have used semi-automated techniques to analyze porosity distribution from microradiograph [11–14] and synchrotron [15] data of cadaveric bone specimens. In vivo quantification of cortical bone microstructure is now possible using high-resolution peripheral quantitative computed tomography (HR-pQCT). This technology permits, for the first time, visualization and quantification of longitudinal changes in cortical porosity. While the resolution of HR-pQCT does not allow for the depiction of cortical porosity at the level of the smallest canals, pores on the order of 100 μmin diameter and larger are detectable [16]. HR-pQCT data provide reproducible and accurate bone microstructure and strength data [16–19]. While cortical microstructure parameters derived from HR-pQCT images have primarily been reported as values averaged over the entire cortical compartment, recent HR-pQCT studies have confirmed that cortical bone microstructure is heterogeneous [20–22] and that regional analysis of cortical bone microstructure increases sensitivity in detecting age-related changes [22].

Characterization of cortical microstructure within concentric layers, or laminar regions, may provide important information about the processes accompanying aging. Identification of micro-structural changes at the endosteal border would clarify longitudinal shifts in trabecular and cortical compartment boundaries [23]. Identification of changes near the periosteal border may detect altered mechanical resistance to bending loads [10,24]. Further, determination of microstructure distributions – and longitudinal changes in distributions – could help to elucidate mechanisms of pore network expansion. For example, a longitudinal increase in porosity concentrated near the endosteal border could indicate a process driven by expansion of the marrow space and ‘trabecularization’ of the cortical compartment, while an increase in porosity that is uniform throughout the cortical compartment could indicate a process driven by expansion of the vascular network. Moreover, determining microstructure

distribution may prove helpful in assessing fracture risk and providing personalized pharmacologic interventions.

The overall goal of this work was to investigate spatial distributions of microstructural changes in the cortical compartment associated with aging in males and females. The specific aims were to: 1) develop an automated technique for laminar analysis of cortical microstructure based on HR-pQCT data, and; 2) apply this technique to explore sex- and age-specific distribution of porosity within the cortex. To address these aims, we evaluated HR-pQCT images of the distal tibia from a cross-sectional cohort of 145 males and females ranging in age from 20 to 78, characterizing detectable pores as being in the endosteal, midcortical, or periosteal layers of the cortical compartment. Metrics describing porosity, pore size, and pore number were quantified within each layer and compared across sexes, age groups, and cortical layers. Laminar analysis of cortical microstructure provides a framework for localizing and characterizing the influence of sex and aging on the cortical pore network.

Methods

Subjects

For this study, baseline examinations from a longitudinal study were considered (Table 1). HR-pQCT image data were acquired from 145 subjects aged 20 to 78 years (92 females, age = 47.8 ± 15.7 years; 53 males, age = 45.5 ± 16.3 years). Of the women aged less than 50, 1 was postmenopausal. This represents 1 of 14 (7%) of the 40–49 year age group. Of the women aged 50 and over, 1 was premenopausal. This represents 1 of 21 (5%) of the 50–59 year age group. The ethnic composition of the subjects reflected the diversity of the San Francisco Bay Area: 47% Caucasian, 44% Asian, 6% Hispanic, and 3% African-American. Ethnic distribution was similar across sexes and age groups. History or evidence of metabolic bone disease, as well as chronic treatment with pharmacological agents affecting bone metabolism were exclusion criteria for this study. The study protocol was approved by the UCSF Committee on Human Research, and all subjects gave written informed consent prior to participation.

HR-pQCT imaging

All subjects were imaged using the XtremeCT HR-pQCT system (Scanco Medical AG, Brüttisellen, Switzerland) using the manufacturer's standard in vivo protocol [25,26]. Two operators acquired the scans, using identical procedures and protocols. For each subject, the ankle was immobilized in a carbon fiber cast fixed within the gantry of the scanner to minimize motion during imaging. The scan region was composed of 110 slices, spanned 9.02 mm in length, and was defined on a single dorsal–palmar projection image of the distal tibia. This region started 22.5 mm from the mid-jointline and extended proximally. For tomography, 750 projections were acquired over 180° with a 100-ms integration time at each angular position. 82-μm voxels were obtained from a 12.6-cm field of view (FOV) reconstructed across a 1536 × 1536 matrix using a modified Feldkamp algorithm [27]. The total scan time was 2.8 min with an equivalent dose of approximately 3 μSv for each site scanned. Images were inspected for motion-related artifacts, and subjects were rescanned if

necessary. All scans included in this study were of quality grading ≤ 2 based on the manufacturer's qualitative grading scheme [28]. A single operator determined the quality grading and performed image analysis.

Cortical segmentation

Initial contours of the cortical compartment were generated using a three-stage semi-automated image processing chain. A detailed discussion of this algorithm has been presented by Burghardt et al. [17]. In the first stage, an autocontouring process identifies the periosteal and endosteal boundaries. Qualitative inspection of the automatically generated contours is performed for quality assurance, and minor adjustments are made where necessary. In the second stage, resolved intracortical porosity is distinguished from other features (e.g., erosions or artefactual surface roughness). In the final stage, the segmented cortical compartment and porosity masks are combined to generate a refined image of the cortical compartment. All image analysis was performed in a customized Image Processing Language (IPL v.506a-ucsf, Scanco Medical AG) that includes in-house functionality.

Separation into three layers

After the initial segmentation, the refined cortical compartment was divided into three laminar layers of equal thickness: the endosteal, midcortical, and periosteal layers (Fig. 1). For each slice, the inner and outer boundaries of the midcortical layer were generated as follows. First, endosteal and periosteal boundaries were discretized. Starting from an initial point on each boundary, each pixel was iteratively recorded in a clockwise direction. Second, every point (X^k_{endo}, Y^k_{endo}) on the endosteal boundary was paired with the closest point on the periosteal boundary (X^k_{peri}, Y^k_{peri}). Note *k* enumerates the number of points on the endosteal boundary. Because the number of discretized points on the periosteal boundary is larger than on the endosteal boundary, not all points on the periosteal boundary are matched. Third, points one-third and two-thirds of the distance d^k between points (X^k_{endo}, Y^k_{endo}) and X^k_{peri}, Y^k_{peri} mark points on the inner and outer boundaries of the midcortical layer, respectively. That is, a point on the inner midcortical boundary was calculated as $\left(X^k_{endo}+{d^k_x}/{3}\,, Y^k_{endo}+{d^k_y}/{3}\right)$ and a point on the outer midcortical boundary as $\left(X^k_{endo}+{2d^k_x}/{3}\,, Y^k_{endo}+{2d^k_y}/{3}\right)$. Finally, continuous midcortical boundaries were generated by performing dilations and erosions to join the discrete midcortical boundary points.

Assignment of pores to layer

Once the cortical compartment was separated into endosteal, midcortical, and periosteal layers, each cortical pore was assigned to a layer using the following procedure (Fig. 1). First, a skeletonization routine deconstructing the cortical pore network into individual elements was applied [29]. Briefly, this skeletonization routine is a medial surface, topology preserving technique based on the MB-3D algorithm of Manzanera et al. [30]. Following skeletonization, each pore element was assigned to a layer according to the location of its

skeleton on a slice-by-slice basis. The entire area of the pore was assigned to the layer in which its skeleton resided, even in the case that some area of the pore crossed a border into a different layer. If the pore element had a planar morphology, or if a tube-like pore was oriented along the slice plane, multiple skeleton points existed for a single pore on a single slice. In this case the center of mass of multiple skeleton points was used to define the pore location.

Quantification of laminar analysis cortical porosity metrics

Within each layer, three metrics to quantify cortical porosity were computed: total pore area (TPA, mm^2/mm^2), total pore number (TPN, mm^{-2}), and average pore area (APA, mm^2). Pore pixels assigned to each layer were summed at each slice and converted to per-slice total pore area. Similarly, individual pores (as determined by the skeletonization algorithm) assigned to each layer were summed at each slice to generate per-slice total pore number. The area of each pore was recorded and per-slice average pore area was calculated for each layer. Both pore area and pore number were then normalized by layer area on a slice-by-slice basis. TPA, TPN, and APA within each layer were then calculated as means across all slices of per-slice total pore area, total pore number, and average pore area, respectively. All laminar analysis calculations were performed in MATLAB (R2012a-Student, The MathWorks, Inc.).

Reproducibility of laminar analysis cortical porosity metrics

To evaluate the reproducibility of the metrics quantified from cortical laminar analysis, existing reproducibility datasets were retrospectively analyzed. The reproducibility scans were performed on 15 female subjects (age = 60 ± 7 years) with two repeat acquisitions at the distal tibia. Scans were included in the analysis if their quality grading did not differ by more than 0.5, based on the grading system devised by the manufacturer [28]. The entire image processing workflow, including cortical segmentation and laminar analysis, was repeated for each data set. Root mean square coefficient of variation (RMSCV) of the paired scans was calculated for each metric of laminar analysis.

Statistical analysis

Mean and standard deviations were calculated for all cortical indices globally and within each layer. Values were calculated for the entire cohort and for subgroups of sex and age. To evaluate age-related trends, participants were grouped by decade as well as divided into young (20–29 years) and elderly (65–78 years) subgroups (sample sizes provided in Table 1). Because Shapiro–Wilk W tests revealed that parameters were not all distributed normally, non-parametric comparison tests were administered. Wilcoxon tests, with Bonferroni correction as appropriate, were used to compare values among layers, between sexes, and across age groups. Statistical analysis comparing values in young vs elderly cohorts was performed on both absolute and percent differences. To test if there were age-related differences in each parameter, as well as to test if these differences varied among layers, analysis of variance (ANOVA) was performed with layer as a within factor and age (grouped into decades) as a between factor. Because the data was unbalanced, post-hoc tests accounting for the unequal variances between groups were performed. For all comparisons, the desired level of statistical significance was set to $\alpha < 0.05$. All reported p-values are

Bonferroni-corrected values $p_{corrected} = Np_{uncorrected}$, where N is the number of comparisons made. All statistical tests were performed using R (v.2.13.0, The R Foundation for Statistical Computing).

Results

Reproducibility of laminar analysis cortical porosity metrics

Reproducibility data are presented in Table 2. RMSCV values for TPA, TPN, and APA within the midcortical layer were similar to previously published RMSCV for Ct.Po (3.9%) in a reproducibility cohort of the same sex and age [17]. Higher RMSCV values were found in the endosteal and periosteal layers, where boundary definition is more influential. Reproducibility in the younger subjects was not quantified. However, because our analysis is applied to the precise pore segmentation described by Burghardt et al. [17] we expect RMSCV values to be higher in the younger group, just as Burghardt et al. found for Ct.Po.

Spatial distribution in the combined cohort

Significant heterogeneity between layers was observed within the cohort considered as a whole. The lowest TPA was found in the periosteal layer, with endosteal and midcortical layers displaying 42% and 43% higher TPA values, respectively ($p < 0.001$ for both comparisons). While no significant difference in TPA between the endosteal and midcortical layers was observed, the nature of the porosity in these layers differed. Endosteal pores were more numerous than midcortical and periosteal pores, with 9% ($p < 0.01$) and 37% ($p < 0.001$) higher TPN values, respectively. In contrast, midcortical pores were larger than endosteal and periosteal pores, with 9% and 23% higher APA, respectively ($p < 0.001$ for both comparisons).

Spatial distribution by age

Spatial distribution of porosity varied with age. When only the young cohort was considered, the endosteal layer displayed the highest TPA, 80% ($p < 0.01$) and 168% ($p < 0.001$) higher than midcortical and periosteal layers, respectively. High endosteal TPA was accompanied by high endosteal TPN, 73% and 117% higher than midcortical and periosteal layers, respectively ($p < 0.001$ for both comparisons). Lower spatial variation was observed in APA within the young cohort; endosteal APA was similar to midcortical APA ($p > 0.05$) and only 21% ($p < 0.001$) higher than the periosteal layer.

In contrast, when only the elderly cohort was considered, the midcortical layer displayed the highest values for all parameters. Midcortical TPA in the elderly cohort was 36% ($p < 0.01$) and 122% ($p < 0.001$) higher than endosteal and periosteal values, respectively. Pores in the midcortical layer were both more numerous and larger than those in other layers. Midcortical TPN was 16% ($p < 0.05$) and 74% ($p < 0.001$) higher than endosteal and periosteal values, and midcortical APA was 14% ($p < 0.05$) and 30% ($p < 0.001$) higher than endosteal and periosteal values.

The elderly cohort displayed higher values than the young cohort for all parameters both globally and within each layer. While all three layers displayed significant age-related

differences in TPA, the midcortical layer was most sensitive to age (+344%, $p < 0.001$). Similarly, the midcortical layer showed the greatest increase with age in both TPN (+243%, $p < 0.001$) and APA (+31%, $p < 0.001$). The endosteal layer showed the least sensitivity to age in all three parameters, with TPA increasing by 81% ($p < 0.001$), TPN by 70% ($p < 0.001$), and APA by 14% ($p < 0.05$). The periosteal layer showed intermediate increases in all three parameters (TPA +198%; TPN +147%; APA +21% all $p < 0.001$). Comparisons among layers hold for both percent and absolute differences between elderly and young cohorts. Global values reflect intermediate increases with age similar to the periosteal values.

Spatial distribution by age and sex

Porosity distribution changes associated with aging varied substantially when considering female and male subjects as separate cohorts (Tables 3 & 4; Fig. 2). The midcortical layer was most sensitive to age for TPA in both females and males. However, the female cohort displayed a 710% ($p < 0.001$) increase midcortically with age (vs. 299% $p < 0.001$ globally), while males displayed a 172% ($p < 0.001$) increase midcortically with age (vs. 118% $p < 0.001$ globally). Females experienced larger changes with age compared to males within the endosteal and periosteal layers as well. Similarly, females displayed greater age-related changes in TPN within every layer. In contrast, females and males displayed comparable small to non-significant changes with age in APA. Comparisons of age-related changes between sexes hold for both percent and absolute differences.

Figs. 3–5 provide a decade-by-decade analysis of age-related changes in males and females for TPA, TPN, and APA. Significant differences between decades were detected in females between the 40–49 group and the 50–59 group. Midcortical TPA was higher in the 50–59 group by 126% ($p < 0.05$). Midcortical and periosteal TPN were higher in the 50–59 group by 128% ($p < 0.001$) and 79% ($p < 0.05$), respectively.

Considering only the young cohort, females displayed lower TPA values than males both globally and within each layer. Female TPA was 22% ($p < 0.05$) lower endosteally, 62% ($p < 0.001$) lower midcortically, and 54% ($p < 0.01$) lower periosteally, compared to 46% ($p < 0.01$) lower globally. In the young group, sex differences in TPA were associated with significant differences in TPN. Female TPN was 33% ($p < 0.05$) lower endosteally, 64% ($p < 0.001$) lower midcortically, and 54% ($p < 0.001$) lower periosteally, compared to 48% ($p < 0.01$) lower globally. No significant sex differences in APA were found globally or within layers.

In contrast, when only the elderly cohort was considered, females displayed lower TPA values only within the periosteal layer (20% lower than males, $p < 0.05$). No significant sex differences in TPN were found globally or within layers. Females displayed lower APA values only within the endosteal layer (16% lower than males, $p < 0.05$).

Discussion

We have developed a technique for the localization and characterization of intracortical pore distribution from in vivo HR-pQCT data. In this study, we demonstrated that considerable

variability exists in the spatial distribution of detectable cortical porosity at the distal tibia, and that this variability is dependent on age and sex. Specifically, we found that endosteal porosity is dominant in young males and females while midcortical porosity is dominant in the elderly, particularly in females. Accordingly, the dramatic acceleration in intracortical porosity documented during aging in women occurs predominantly in the midcortical layer. Intracortical pore distribution analysis may provide insight into differential mechanisms of pore network expansion as well as biomechanical consequences of pore distribution.

Our results confirm that cortical porosity increases with age, consistent with earlier reports [31,32]. Porosity increases more dramatically with age in women than in men, with the largest increase occurring during the early post-menopausal decade. The results of this study localize this dramatic increase in detectable porosity to the midcortical layer. This outcome is of course dependent on boundary definitions. The endocortical boundary definition used in this analysis may exclude zones of trabecularized cortex, particularly in elderly subjects [23]. Excluding these zones means that we are limited to evaluating intracortical porosity distribution within the compact cortex. This approach provides conservative estimates of porosity near the endosteal border. This approach may also result in the analysis of nonhomologous layers when comparing young versus elderly subjects; the periosteal and midcortical layers of the elderly individual may correspond to the periosteal layer (alone) of the younger individual. However, the laminar analysis technique described here could certainly be applied with alternate endosteal boundary definitions. In a longitudinal study the baseline endosteal boundary could be mapped forward to the follow-up time-points to examine the role of endocortical trabecularization on pore distribution [33,34].

Our finding of elevated midcortical porosity in elderly females contradicts microradiography studies conducted on bone samples from the femoral diaphysis [9,12], which found increasing gradients of porosity from the periosteum to the endosteum in young and elderly males and females. The inconsistency in findings could be due to two important differences between these anatomic sites. First, endosteal boundary morphology differs between these sites. At the distal tibia metaphysis large pores at the endosteal surface may merge into the trabecularized zone over time and therefore be excluded from laminar analysis of the intracortical region, as described above. At the femoral diaphysis this effect is less likely. Second, sexual dimorphism differs between these sites, evidenced by the fact that females display higher cortical porosity than males at the femur [12,35,36] in contrast to the trend observed at the tibia in our study and others [31,32]. Additionally, the contradiction in results could be influenced by differences in the scale of porosity detected. In this HR-pQCT study detectable porosity includes large osteonal canals or resorption cavities, but excludes the smallest pores. The microradiography studies, in contrast, detect smaller pores. Large and small pores may differ in spatial distribution and progression.

Increased porosity can be driven by increased number of pores, increased size of pores, or both. Our results suggest that at the tibia, age-related porosity increase is driven primarily by pore number rather than pore size. This is in agreement with some ex-vivo studies [37,38], but contradictory to others [14,35]. Again, it is important to note that the current study evaluates a different anatomic site and different scale of porosity compared to published ex vivo studies. It is likely that unique biological processes drive porosity at these various sites

and length-scales. It is also possible that, due to the limited resolution of HR-pQCT, increased pore number in elderly subjects is actually reflective of small pores enlarging to the detection threshold. This phenomenon may be biasing our interpretation of relative trends in pore number and size. The laminar analysis workflow can be applied to higher-resolution images, for example those acquired by micro-computed tomography. A high resolution ex vivo study of distal tibia specimens from donors of a range of ages would provide insight into these questions.

Spatial distribution of intracortical porosity may provide insight into differential mechanisms of pore network expansion. In a recent study evaluating the development of pathological porosity during a period of disuse [39], we found that porosity increased uniformly throughout the cortex. In contrast, the results of this cross-sectional study indicate that age-related increases in porosity are most extreme in the midcortical layer. We hypothesize that unique processes of pore network expansion are acting in disuse versus aging, which are reflected in the spatial distribution of cortical pores.

Spatial distribution of porosity may also reveal important biomechanical characteristics. As detailed by Burr [24], the relationship between porosity and stiffness or strength under a bending load depends heavily on the distribution of porosity. Pores located in the endosteal layer will have a less detrimental effect than those located in the midcortical or periosteal layer. Accordingly, Squillante and Williams reported elevated periosteal relative to endosteal porosity in the femoral neck cortex of elderly fracture patients but not of elderly non-fracture patients [10]. While the data in this work are limited to the distal tibia, the laminar analysis technique presented here may be applied to other cortical regions, including those experiencing primarily bending loads. Computational and biomechanical validation is necessary to determine the utility of HR-pQCT-based pore distribution metrics in predicting biomechanical properties.

The results presented here must be interpreted in the context of three important limitations. First, as noted above, HR-pQCT scanning cannot resolve pores smaller than approximately 100 μm in diameter. The measures described in this manuscript are directly derived from the pore segmentation previously described in the literature [16,17,22, 40]. This pore segmentation has been validated by ex vivo studies that found good agreement between HR-pQCT and higher resolution micro-CT (μCT) quantification of porosity [16,41]. Second, this work relies on a cross-sectional rather than longitudinal study design. Third, sample sizes – in particular for sex-specific comparisons – are small and therefore our findings should be confirmed through a larger population-based study.

In conclusion, we have demonstrated the existence of significant variability in the amount of porosity and structure of the pore network in the cortex of the tibia. The laminar analysis technique allows for localization of pores to one of three cortical layers: endosteal, midcortical, or periosteal. Furthermore, pore characteristics are analyzed to determine whether porosity is driven primarily by pore number or pore size. Quantification of these parameters within each layer provides increased sensitivity in analyzing sex- and age-related differences in the cortical pore network and motivates hypotheses around the mechanisms of porosity development. Laminar analysis may be an important step towards providing more

personalized pharmacologic interventions, particularly in understanding the underlying pathophysiology behind pathological porosity and bone fragility.

Acknowledgments

This work was funded by the National Institutes of Health Grants K01 AR056734 and NIH R03 AR064004 (GJK), R01 AG017762 (SM), and R01 AR060700 (AJB). Support for JAN was provided by UC Berkeley Integrative Graduate Education and Research Traineeship DGE-0903711 through the Center for Interdisciplinary Bio-Inspiration in Education and Research (CiBER-IGERT). Support for KPC was provided by the Qualcomm Undergraduate Experiences in Science and Technology (QUEST) program.

References

1. Currey JD. The effect of porosity and mineral content on the Young's modulus of elasticity of compact bone. J Biomech. 1988; 21(2):131–9. [PubMed: 3350827]
2. Schaffler MB, Burr DB. Stiffness of compact bone: effects of porosity and density. J Biomech. 1988; 21(1):13–6. [PubMed: 3339022]
3. Ural A, Vashishth D. Effects of intracortical porosity on fracture toughness in aging human bone: a microCT-based cohesive finite element study. J Biomech Eng. 2007; 129(5):625–31. [PubMed: 17887887]
4. Nicks KM, Amin S, Atkinson EJ, Riggs BL, Melton JL, Khosla S. Relationship of age to bone microstructure independent of areal bone mineral density. J Bone Miner Res. 2012; 27(3):637–44. [PubMed: 22095490]
5. Hui SL, Slemenda CW, Johnston CC Jr. Age and bonemass as predictors of fracture in a prospective study. J Clin Invest. 1988; 81(6):1804–9. [PubMed: 3384952]
6. Bala Y, Zebaze R, Ghasem-Zadeh A, Atkinson EJ, Iuliano S, Peterson JM, et al. Cortical porosity identifies women with osteopenia at increased risk for forearm fractures. J Bone Miner Res. 2014; 29(6):1356–62. [PubMed: 24519558]
7. Cooper DM, Turinsky AL, Sensen CW, Hallgrimsson B. Quantitative 3D analysis of the canal network in cortical bone by micro-computed tomography. Anat Rec B New Anat. 2003; 274(1): 169–79. [PubMed: 12964207]
8. Britz HM, Jokihaara J, Leppanen OV, Jarvinen TL, Cooper DM. The effects of immobilization on vascular canal orientation in rat cortical bone. J Anat. 2012; 220(1):67–76. [PubMed: 22050694]
9. Atkinson PJ. Changes in resorption spaces in femoral cortical bone with age. J Pathol Bacteriol. 1965; 89:173–8. [PubMed: 14263459]
10. Squillante RG, Williams JL. Videodensitometry of osteons in females with femoral neck fractures. Calcif Tissue Int. 1993; 52(4):273–7. [PubMed: 8467407]
11. Stein MS, Feik SA, Thomas CD, Clement JG, Wark JD. An automated analysis of intracortical porosity in human femoral bone across age. J Bone Miner Res. 1999; 14(4):624–32. [PubMed: 10234585]
12. Bousson V, Meunier A, Bergot C, Vicaut E, Rocha MA, Morais MH, et al. Distribution of intracortical porosity in human midfemoral cortex by age and gender. J Bone Miner Res. 2001; 16(7):1308–17. [PubMed: 11450707]
13. Thomas CD, Feik SA, Clement JG. Regional variation of intracortical porosity in the midshaft of the human femur: age and sex differences. J Anat. 2005; 206(2):115–25. [PubMed: 15730477]
14. Thomas CD, Feik SA, Clement JG. Increase in pore area, and not pore density, is the main determinant in the development of porosity in human cortical bone. J Anat. 2006; 209(2):219–30. [PubMed: 16879600]
15. Chappard C, Bensalah S, Olivier C, Gouttenoire PJ, Marchadier A, Benhamou C, et al. 3D characterization of pores in the cortical bone of human femur in the elderly at different locations as determined by synchrotron micro-computed tomography images. Osteoporos Int. 2013; 24(3): 1023–33. [PubMed: 22814943]

16. Tjong W, Kazakia GJ, Burghardt AJ, Majumdar S. The effect of voxel size on high-resolution peripheral computed tomography measurements of trabecular and cortical bone microstructure. Med Phys. 2012; 39(4):1893–903. [PubMed: 22482611]
17. Burghardt AJ, Buie HR, Laib A, Majumdar S, Boyd SK. Reproducibility of direct quantitative measures of cortical bone microarchitecture of the distal radius and tibia by HR-pQCT. Bone. 2010; 47(3):519–28. [PubMed: 20561906]
18. MacNeil JA, Boyd SK. Accuracy of high-resolution peripheral quantitative computed tomography for measurement of bone quality. Med Eng Phys. 2007; 29(10):1096–105. [PubMed: 17229586]
19. Macneil JA, Boyd SK. Bone strength at the distal radius can be estimated from high-resolution peripheral quantitative computed tomography and the finite element method. Bone. 2008; 42(6): 1203–13. [PubMed: 18358799]
20. Mueller TL, van Lenthe GH, Stauber M, Gratzke C, Eckstein F, Muller R. Regional, age and gender differences in architectural measures of bone quality and their correlation to bone mechanical competence in the human radius of an elderly population. Bone. 2009; 45(5):882–91. [PubMed: 19615477]
21. Boyd SK. Site-specific variation of bone micro-architecture in the distal radius and tibia. J Clin Densitom. 2008; 11(3):424–30. [PubMed: 18280194]
22. Kazakia GJ, Nirody JA, Bernstein G, Sode M, Burghardt AJ, Majumdar S. Age- and gender-related differences in cortical geometry and microstructure: improved sensitivity by regional analysis. Bone. 2013; 52(2):623–31. [PubMed: 23142360]
23. Zebaze RM, Ghasem-Zadeh A, Bohte A, Iuliano-Burns S, Mirams M, Price RI, et al. Intracortical remodelling and porosity in the distal radius and post-mortem femurs of women: a cross-sectional study. Lancet. 2010; 375(9727):1729–36. [PubMed: 20472174]
24. Burr DB. Cortical bone: a target for fracture prevention? Lancet. 2010; 375(9727):1672–3. [PubMed: 20472154]
25. Kazakia GJ, Hyun B, Burghardt AJ, Krug R, Newitt DC, de Papp AE, et al. In vivo determination of bone structure in postmenopausal women: a comparison of HR-pQCT and high-field MR imaging. J Bone Miner Res. 2008; 23(4):463–74. [PubMed: 18052756]
26. Boutroy S, Bouxsein ML, Munoz F, Delmas PD. In vivo assessment of trabecular bone microarchitecture by high-resolution peripheral quantitative computed tomography. J Clin Endocrinol Metab. 2005; 90(12):6508–15. [PubMed: 16189253]
27. Laib A, Hauselmann HJ, Ruegsegger P. In vivo high resolution 3D-QCT of the human forearm. Technol Health Care. 1998; 6(5–6):329–37. [PubMed: 10100936]
28. Pialat JB, Burghardt AJ, Sode M, Link TM, Majumdar S. Visual grading of motion induced image degradation in high resolution peripheral computed tomography: impact of image quality on measures of bone density and micro-architecture. Bone. 2012; 50(1):111–8. [PubMed: 22019605]
29. Tjong W, Nirody J, Burghardt AJ, Carballido-Gamio J, Kazakia GJ. Structural analysis of cortical porosity applied to HR-pQCT data. Med Phys. 2014; 41(1)
30. Manzanera, A.; Bernard, TM.; Preteux, F.; Longuet, B. Medial faces from a concise 3D thinning algorithm proceeds of the 7th IEEE International Conference on Computer Vision; 1999; p. 337-43.
31. Burghardt AJ, Kazakia GJ, Ramachandran S, Link TM, Majumdar S. Age- and gender-related differences in the geometric properties and biomechanical significance of intracortical porosity in the distal radius and tibia. J Bone Miner Res. 2010; 25(5):983–93. [PubMed: 19888900]
32. Macdonald HM, Nishiyama KK, Kang J, Hanley DA, Boyd SK. Age-related patterns of trabecular and cortical bone loss differ between sexes and skeletal sites: a population-based HR-pQCT study. J Bone Miner Res. 2011; 26(1):50–62. [PubMed: 20593413]
33. Tjong, W.; Burghardt, A.; Patsch, JM.; Majumdar, S.; Kazakia, G. The effect of image registration and endocortical segmentation methods on longitudinal HR-pQCT analysis of cortical bone quality. American Society for Bone and Mineral Research; Minneapolis, MN: 2012.
34. Nishiyama KK, Pauchard Y, Nikkel LE, Iyer S, Zhang C, McMahon DJ, et al. Longitudinal HR-pQCT and image registration detects endocortical bone loss in kidney transplantation patients. J Bone Miner Res. 2014; 30(3):456–63.

35. Cooper DM, Thomas CD, Clement JG, Turinsky AL, Sensen CW, Hallgrimsson B. Age-dependent change in the 3D structure of cortical porosity at the human femoral midshaft. Bone. 2007; 40(4): 957–65. [PubMed: 17223618]

36. Chen H, Zhou X, Shoumura S, Emura S, Bunai Y. Age- and gender-dependent changes in three-dimensional microstructure of cortical and trabecular bone at the human femoral neck. Osteoporos Int. 2010; 21(4):627–36. [PubMed: 19543764]

37. Currey JD. Some effects of ageing in human Haversian systems. J Anat. 1964; 98:69–75. [PubMed: 14109815]

38. Martin RB, Pickett JC, Zinaich S. Studies of skeletal remodeling in aging men. Clin Orthop Relat Res. 1980; 149:268–82. [PubMed: 7408312]

39. Kazakia GJ, Tjong W, Nirody JA, Burghardt AJ, Carballido-Gamio J, Patsch JM, et al. The influence of disuse on bone microstructure and mechanics assessed by HR-pQCT. Bone. 2014; 63C:132–40. [PubMed: 24603002]

40. Buie HR, Campbell GM, Klinck RJ, MacNeil JA, Boyd SK. Automatic segmentation of cortical and trabecular compartments based on a dual threshold technique for in vivo micro-CT bone analysis. Bone. 2007; 41(4):505–15. [PubMed: 17693147]

41. Nishiyama KK, Macdonald HM, Buie HR, Hanley DA, Boyd SK. Postmenopausal women with osteopenia have higher cortical porosity and thinner cortices at the distal radius and tibia than women with normal aBMD: an in vivo HR-pQCT study. J Bone Miner Res. 2010; 25(4):882–90. [PubMed: 19839766]

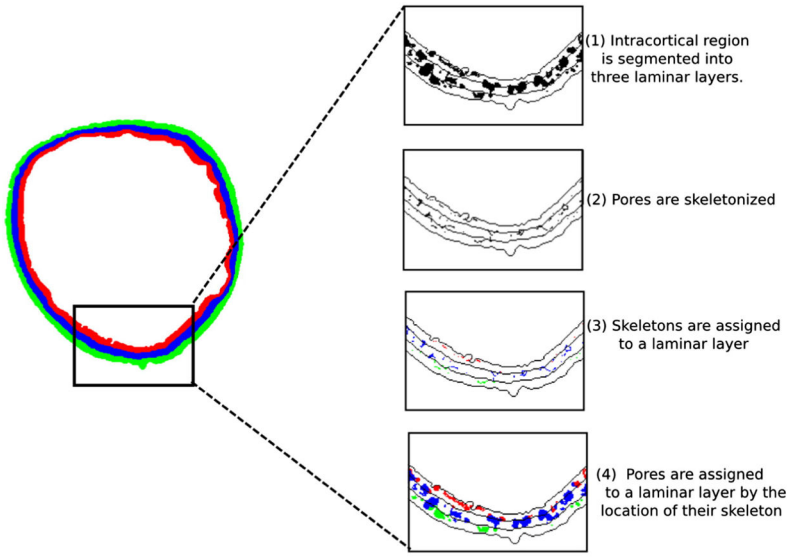

Fig. 1.

An overview of cortical layers and the pore assignment technique. Unassigned pores are shown in black (top panel in inlay). Pores are assigned to one of endosteal, midcortical, or periosteal layers (shown in red, blue, and green respectively). This assignment is done according to the location of the pore's skeleton (second and third panels in inlay). Pores are assigned wholly to a layer; no individual pore is split between layers (bottom panel in inlay). (For interpretation of the references to color in this figure legend, the reader is referred to the web version of this article.)

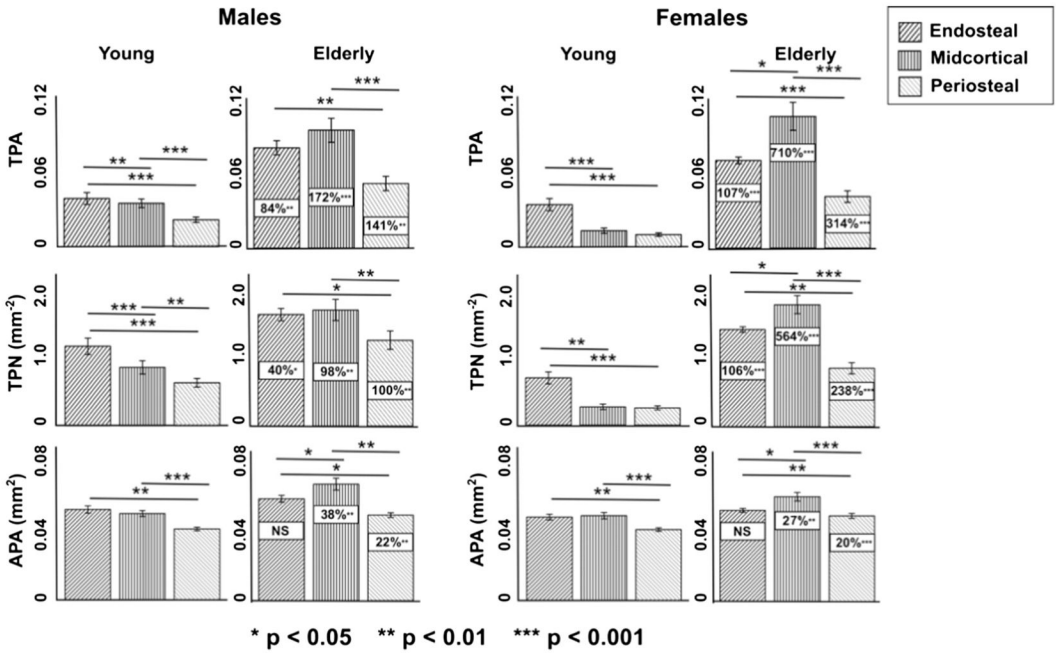

Fig. 2.

Gender-specific variation in the evolution of total pore area (TPA, mm^2/mm^2), total pore number (TPN, mm^{-2}), and average pore area (APA, mm^2) with age. Data shown are mean ± 95% CI in each cohort grouped by age and gender. Boxed values indicate differences between young (20–29) and elderly (65–78) cohorts.

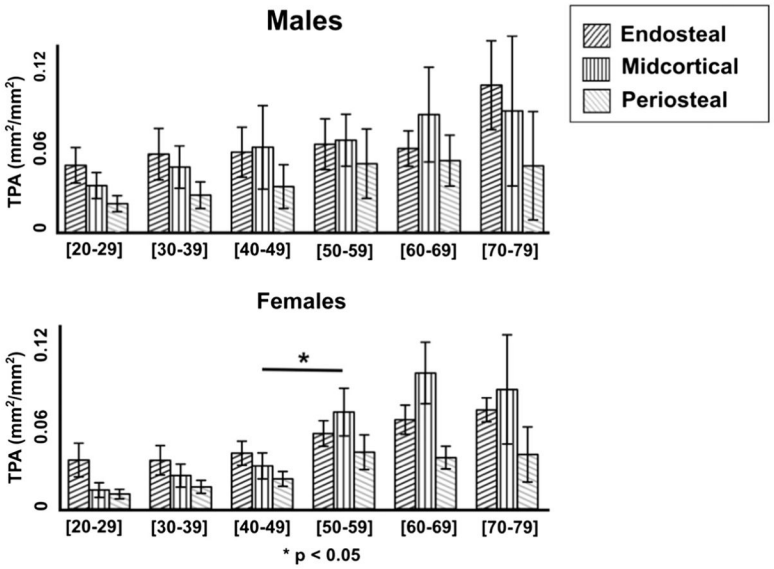

Fig. 3.

Decade-by-decade total pore area (TPA, mm^2/mm^2) by layer for males (top) vs. females (bottom). Data shown are the mean ± 95% CI. Females display a significant increase in porosity between the fourth and fifth decades (consistent with the onset of menopause), while males show a more gradual increase. Accelerated age-related porosity increase is most extreme in the midcortical layer in the female cohort.

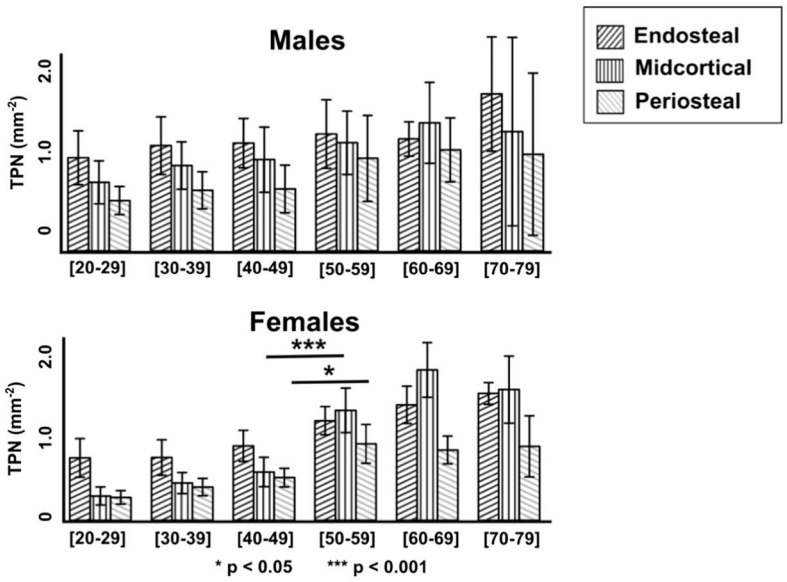

Fig. 4.

Decade-by-decade analysis of total pore number (TPN, mm^{-2}) by layer for males (top) vs. females (bottom). Data shown are the mean ± 95% CI. The female cohort undergoes a more drastic increase in TPN with age than the male cohort. Age-related TPN increase is most extreme in the midcortical layer in the female cohort.

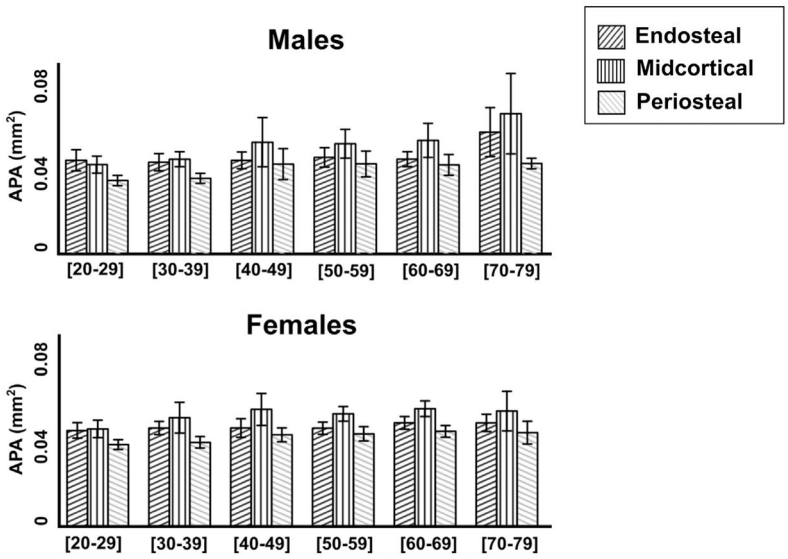

Fig. 5.

Decade-by-decade analysis of average pore area (APA mm^2) by layer for males (top) vs. females (bottom). Data shown are the mean ± 95% CI.

Table 1

Summary of subject numbers by sex and age group. The study consisted of 145 volunteers (92 females/53 males). Subject ages ranged from 20 to 78 years. All subjects were scanned at the tibia.

	Decade						Young	Elderly
Sex	**20–29**	**30–39**	**40–49**	**50–59**	**60–69**	**70–78**	**20–29**	**65–78**
Female	16	16	14	21	18	7	16	13
Male	13	13	5	11	8	3	13	9

Table 2

Reproducibility (RMSCV) of cortical porosity laminar analysis metrics.

	RMS-CV (%)
TPA	
Endosteal	9.35
Midcortical	3.82
Periosteal	6.09
TPN	
Endosteal	6.42
Midcortical	3.04
Periosteal	5.27
APA	
Endosteal	5.77
Midcortical	3.94
Periosteal	4.37

Table 3

Global and regional TPA, TPN, and APA for the entire female cohort, the young female cohort (20–29), and the elderly female cohort (65–78). All table entries report means ± SEM.

Females		TPA mm^2/mm^2	TPN mm^{-2}	APA mm^2
Entire cohort	Endosteal	0.045 ± 0.002	1.012 ± 0.05	0.043 ± 0.001
	Midcortical	0.049 ± 0.005	0.955 ± 0.08	0.048 ± 0.001
	Periosteal	0.026 ± 0.002	0.613 ± 0.04	0.039 ± 0.001
	Global	0.039 ± 0.003	0.826 ± 0.05	0.045 ± 0.001
Young cohort	Endosteal	0.033 ± 0.006	0.721 ± 0.12	0.041 ± 0.002
	Midcortical	0.013 ± 0.003	0.280 ± 0.06	0.042 ± 0.003
	Periosteal	0.010 ± 0.002	0.264 ± 0.04	0.035 ± 0.001
	Global	0.017 ± 0.003	0.397 ± 0.05	0.041 ± 0.001
Elderly cohort	Endosteal	0.068 ± 0.003	1.481 ± 0.05	0.046 ± 0.001
	Midcortical	0.102 ± 0.012	1.860 ± 0.15	0.053 ± 0.003
	Periosteal	0.040 ± 0.005	0.891 ± 0.09	0.042 ± 0.002
	Global	0.069 ± 0.006	1.374 ± 0.08	0.049 ± 0.002

Table 4

Global and regional TPA, TPN, and APA for the entire male cohort, the young male cohort [20–29], and the elderly male cohort (65–78). All table entries report means ± SEM.

Males		TPA mm^2/mm^2	TPN mm^{-2}	APA mm^2
Entire cohort	Endosteal	0.059 ± 0.004	1.248 ± 0.08	0.044 ± 0.001
	Midcortical	0.057 ± 0.005	1.088 ± 0.09	0.049 ± 0.001
	Periosteal	0.035 ± 0.004	0.837 ± 0.08	0.039 ± 0.001
	Global	0.048 ± 0.003	0.999 ± 0.07	0.047 ± 0.001
Young cohort	Endosteal	0.048 ± 0.007	1.068 ± 0.16	0.045 ± 0.002
	Midcortical	0.034 ± 0.005	0.786 ± 0.13	0.042 ± 0.002
	Periosteal	0.021 ± 0.003	0.577 ± 0.09	0.035 ± 0.001
	Global	0.032 ± 0.004	0.767 ± 0.11	0.042 ± 0.002
Elderly cohort	Endosteal	0.078 ± 0.008	1.496 ± 0.12	0.046 ± 0.001
	Midcortical	0.091 ± 0.014	1.559 ± 0.21	0.049 ± 0.002
	Periosteal	0.050 ± 0.008	1.152 ± 0.18	0.040 ± 0.001
	Global	0.070 ± 0.008	1.334 ± 0.07	0.053 ± 0.003